TOWARDS A COMPUTATIONAL FLUID DYNAMICS METHODOLOGY FOR STUDIES OF LARGE SCALE LNG RELEASES

Jens A. Melheim[1]*, Mathieu Ichard[1] and Marco Pontiggia[2]
[1]GexCon AS, Fantoftvegen 38, NO-5893 Bergen, Norway
[2]Politecnico di Milano, Dip. di Chimica, Materiali e Ingegneria Chimica "G. Natta", via Mancinelli 7, 20131-Milano, Italy

An increasing amount of liquefied natural gas (LNG) is transported by ship and handled at terminals, which often are located near densely populated regions. Released LNG evaporates quickly and a burnable gas cloud is formed near the ground. Size, shape and location of the gas cloud are important parameters for the outcome of eventual events. In risk analysis, the set of gas clouds that might occur should be based on 'known' variables such as weather data, leakage statistics, the geometry etc. Consequently, the quality of the risk analysis depends on the quality of the modelling of LNG spill motion and evaporation, wind conditions, geometry including terrain and the behaviour of cold gas in the wind field. In the present work, a two-dimensional transient spill model is solved simultaneously with a three-dimensional transient flow for the wind. Effort is given to modelling of the heat transfer between the spill and the substrate which determines the evaporation rate. The flow field is modelled by the Reynolds Averaged Navier-Stokes equations that are closed by the standard k-epsilon turbulence model. Proper wind boundary conditions are applied by using the Monin-Obukhov similarity theory. Together, this constitutes a powerful approach where irregular spill shapes, multiple ground properties, and realistic geometries and wind fields can be handled. The Burro and Coyote test series are simulated using this new methodology. The predicted downwind gas concentrations are found to be in good agreement with experimental observations. The effects of atmospheric boundary layer stability as well as terrain representation are also discussed.

INTRODUCTION

In the last ten years, rising interest has been showed in the introduction of new, environmental sustainable energy sources in order to reduce overall pollutants production, and of new energy vectors that allow for lower noxious emissions in towns and cities, where the high population density should increase their negative effects (European Commission, 2002). Major concern has been dedicated to natural gas, which grants a cleaner combustion in respect with traditional fuels, leading to a significant increase in the transported amount and to the realization of new infrastructures for the distribution. Since its low molecular density in the gas phase, natural gas is usually liquefied for economical transportation and storage (Carson, 1994). As a consequence, proper terminals, namely regasifiers, are needed to handle liquefied natural gas (LNG) before its employment. Necessarily, these plants are often located near densely populated zone, leading also to a negative public opinion impact.

The liquefaction is accomplished at significant low temperatures, together with high pressure application. Accidental releases of LNG in those extreme conditions, lead to cryogenic leaks, usually with pool formation. Depending on many factors, such as spilled amount, atmospheric conditions, geometrical features of the spill area, ignition points etc., and an accidental release of LNG can result in different physical phenomena such as jet fire, BLEVE or vapour cloud explosion (Deaves, 1992).

*Corresponding author: e-mail: jens@gexcon.com, tel. +47 41215517, fax. +47 55574331.

In risk analysis, accurate predictions of the size, shape, concentration and location of the gas cloud are needed in order to establish the involved physical phenomenon for the realization of appropriate mitigation and/or prevention systems. Nowadays integral models, such as DEGADIS, SLAB, UDM, are widely used in risk assessment, since they are simple to use and low-time consuming (Havens, 1998; Bernatik, 2004). However, these tools solve simplified one-dimensional flow field equations, introducing semi-empirical relations in order to model features lost due to the problem reduction. Since parameters are fitted on experimental releases data, integral models are strongly influenced by the experimental set up, and these tools should not be used outside the range for which they are optimized. In particular, available field data are obtained in open field or in very simple geometries. As a consequence, for the simulation of scenarios involving complex geometries more powerful tools are required.

The increase in computer performances has made computational fluid dynamics (CFD) a valuable tool in risk assessment. CFD is based on the fully transient three-dimensional solution of the flow field and, therefore, allows for a complete analysis of the geometry effects. LNG dispersion simulations have been conducted and good accuracy has been obtained by using CFD (Hightower, 2004; Hansen, 2007). Nevertheless, some issues, such as pool formation and evaporation, atmospheric stability effects on gas dispersion, terrain influence and so on, still remain open.

Pool evaporation represents the source term of the hazardous gas within the simulated domain. In CFD

simulations, it is usually represented by a convective and/or diffusive flux from an imaginary pool surface. The pool surface and the evaporation rate, depending upon the conditions of the release, are considered to be constant (Gavelli, 2008) or to be evaluated from external model and then introduced in the CFD code through user-defined functions (Sklavounos, 2005). As a consequence of the mentioned approaches, simplified models for the pool features evaluation are used; namely static pool model or circular/annular pool model. Terrain features, such as slopes, irregular bond etc., are not considered in the pool formation process and is possibly leading to severe loss of information.

In this work, FLACS (GexCon, 2009) has been used for Burro and Coyote field tests series simulations. These are LNG releases onto a water pond. FLACS is a CFD tool that solves the Reynolds Averaged Navier-Stokes equations for the flow field, closed by the standard k-ε turbulence model. Atmospheric stratification has taken into account imposing proper boundary profiles at the wind inlet boundary. Wind speed, temperature, turbulent kinetic energy, k, and turbulent dissipation rate, ε, profiles are evaluated accordingly to the Monin-Obukhov similarity theory, as a function of atmospheric parameters, wind speed and temperature at reference height, surface roughness, stability class, solar radiation, and ground heat flux. Moreover, the code has been improved in order to solve a two-dimensional transient spill simultaneously with the three-dimensional transient flow for the wind. The coupling of the pool model with the flow simulation allows a continuous interaction of the two models, leading to a two directional, uninterrupted flux of information between the two phases. Pool shape, dimension and evaporation rate are therefore fully influenced by the geometry of the spill area and by the wind flow field, leading to a different, more physical, behaviour for the same spill in open field or in a confined area. On the other hand, gas evaporated from the pool, as well as heat exchange between liquid and gaseous phase, influences the flow field, creating positive and/or negative buoyancy zones that alter wind turbulence.

THEORY

This section describes the models for the spill and wind imposed at the boundary of the domain that are implemented in the CFD tool FLACS. FLACS solves the governing equations for the flow in time on a staggered Cartesian grid using second order schemes for the spatial discretisation.

SPILL MODELLING

A liquid will spread until it reaches a steady state where the evaporation rate balances the leak or obstacles hinder further pool spread. An LNG spill is driven by gravitational forces in form of differences in the spill height and the shape of the ground. Friction forces resist the motion. For LNG spills, the effect of surface tension can be neglected. The spill motion can be described mathematically by the shallow water equations (Toro, 2001). Brandeis & Ermak (1983) and Woodward (1990) showed that shallow water equation could describe LNG spills on annular grids. In this work, the shallow water equations are solved on a Cartesian grid.

The equation solved for the spill height is given by:

$$\frac{\partial h}{\partial t} + \frac{\partial h u_i}{\partial x_i} = \frac{\dot{m}_L - \dot{m}_V}{\rho_l} \tag{1}$$

and the momentum equation is written as:

$$\frac{\partial u_i}{\partial t} + u_j \frac{\partial u_i}{\partial x_j} = F_{g,i} + F_{\tau,i}, \tag{2}$$

where the gravity term is modelled as follows:

$$F_{g,i} = g\Delta \frac{\partial (h+z)}{\partial x_i}, \tag{3}$$

where also the elevation of the ground has been included. The parameter Δ equals one for spills on solid surfaces and $\Delta = (1 - \rho_l/\rho_w)$ for spills on water. The shear stress between the spill and substrate is given by the general formula:

$$F_{\tau,i} = \frac{1}{8} f_f u_i |\vec{u}| \tag{4}$$

where the expression for the friction factor is estimated as follows:

$$f_{f,\text{lam}} = \frac{64}{4\text{Re}_h}$$

$$f_{f,\text{turb}} = \begin{cases} \left\{ -1.8 \log\left(\frac{1.72}{\text{Re}_h} + \left(\frac{\varepsilon_g}{12\,h} \right)^{1.11} \right) \right\}^{-2} & \text{if } \frac{\varepsilon_g}{h} < 0.2 \\ 0.125 \left(\frac{\varepsilon_g}{h} \right)^{1/3} & \text{if } \frac{\varepsilon_g}{h} \geq 0.2 \end{cases}$$

$$f_f = \max(f_{f,\text{lam}}, f_{f,\text{turb}}) \tag{5}$$

where ε_g is the ground roughness. The interfacial friction between the spill and water is less than the friction on solid grounds. This is particular true when there is a gaseous film between the water and the spill liquid. The GASP code uses a smaller laminar friction coefficient for spill on water (Bosch & Weterings, 2005), which also limits the maximum friction coefficient. We have adapted this approach, and hence the laminar friction factor for spills on water is given by:

$$f_{f,\text{lam,water}} = \frac{12}{4\text{Re}_h} \tag{6}$$

The transport equation for the specific enthalpy reads:

$$\frac{\partial \theta}{\partial t} + u_i \frac{\partial \theta}{\partial x_i} = \frac{\dot{m}_L}{h}(\theta_L - \theta) + \dot{q}_c + \dot{q}_{rad} + \dot{q}_g + \dot{q}_{evap} \quad (7)$$

The first term on the right hand side is due to the leak, $\dot{q}_c$ is convective heat transfer, $\dot{q}_{rad}$ is heat transfer to the pool from radiation, $\dot{q}_g$ is heat transfer to the pool from the substrate, and $\dot{q}_{evap}$ is heat loss due to evaporation. Heat transported to the pool from the ground dominates the heat transfer to the pool for LNG at the boiling point on solid ground or water. Furthermore, the evaporation heat will balance the heat from the ground such that the liquid temperature remains at the boiling point temperature.

Heat transfer from solid and rough grounds (soil and concrete) is approximated by:

$$\dot{q}_{q,solid} = \begin{cases} \dfrac{\lambda_g(T_g^0 - T_l)(1.5 - 0.25(t - t_{gw}))}{\sqrt{\pi \alpha_g}} & \text{if } t < 4\,\text{sec.} \\ \dfrac{\lambda_g(T_g^0 - T_l)}{\sqrt{\pi \alpha_g (t - t_{gw})}} & \text{if } t \geq 4\,\text{sec.} \end{cases} \quad (8)$$

In equation (8), λ_g is the thermal conductivity of the ground, α_g is the thermal diffusivity of the ground and t_{gw} is the time at which the ground is wetted. Infinite ground is assumed in the derivation of the expressions for the heat transferred from the ground in equation (8). Boiling LNG on water can take place in transition boiling and film boiling regimes. Conrado and Vesovic (2000) proposed correlations for film and transition boiling for non-moving liquids. Experiments have shown that the heat transfer coefficient is considerable higher for LNG on the sea than estimated by the correlations for non-moving pools. Hissong (2007) introduced a turbulence factor to model the film instability and the increased contact area between LNG and the sea. In the present work, the local Reynolds number is used to calculate the effective heat transfer rate:

$$\dot{q}_{g,water} = \begin{cases} \dot{q}_{\text{film}}, & \text{if } \mathrm{Re}_h < 15 \\ \dfrac{1}{2}\dot{q}_{\text{film}} + \dfrac{1}{2}\left(\dot{q}_{\text{film}}\left(\dfrac{1500 - \mathrm{Re}_h}{1485}\right) + \dot{q}_{cb}\left(\dfrac{\mathrm{Re}_h - 15}{1486}\right)\right), & \text{if } 15 < \mathrm{Re}_h < 1500 \\ \dfrac{1}{2}\dot{q}_{\text{film}} + \dfrac{1}{2}\dot{q}_{cb}\ , & \text{if } \mathrm{Re}_h > 1500 \end{cases} \quad (9)$$

where $\dot{q}_{\text{film}}$ refers to the heat transfer for non-moving liquids calculated by the correlations in Conrado & Vesovic (2000) and $\dot{q}_{cb}$ is the convective heat transfer that is calculated as follows:

$$\dot{q}_{cb} = 0.0133 \mathrm{Re}_h^{0.69} \mathrm{Pr}_l^{0.4} \frac{\lambda_l}{h}(T_W - T_l) \quad (10)$$

The governing equations for the spill are discretised on a non-uniform Cartesian staggered grid in two dimensions with a finite volume method. A first-order upwind scheme is employed for the convective terms in the momentum equation and a central difference scheme is used for the enthalpy equation. The equations are solved explicitly in time with a 3th order Runge-Kutta solver.

WIND MODELLING

FLACS solves the Reynolds Averaged Navier-Stokes closed by the k-ε model with the standard set of constants (Launder & Spalding, 1974). The atmospheric boundary layer is modelled by forcing profiles for velocity, temperature and turbulence parameters on inlet boundaries. Wind inlet profiles relays on the Monin-Obukhov length L and the atmospheric roughness length z_0. The Monin-Obukhov length can be estimated from measurements and it is positive for stable atmospheric boundary layers, negative for unstable boundary layers and infinity for neutral boundary layers. In risk assessment studies, the Monin-Obukhov length is generally not know and must be guessed, for instance by using the dominant or most hazardous Pasquill stability class and Golder graphs (Bosch, 2005).

The inlet velocity profile is logarithmic and can be written as:

$$U(z) = \frac{u_*}{\kappa}\left(\ln\left(\frac{z + z_0}{z_0}\right) - \psi_m\right) \quad (11)$$

where the friction velocity u^* is given by:

$$u_* = \frac{U_0 \kappa}{\ln\left(\dfrac{z_{ref}}{z_0}\right) - \psi_m} \quad (12)$$

where U_0 is the velocity at the reference height z_{ref}. ψ_m is given by (Bosch, 2005; Ulden, 1985):

$$\psi_m = \begin{cases} 2\ln\left(\dfrac{1+\xi}{2}\right) + \ln\left(\dfrac{1+\xi^2}{2}\right) - 2\arctan(\xi) + \dfrac{\pi}{2} & \text{for } L < 0 \\ -17\left(1 - \exp\left(-0.29\dfrac{z}{L}\right)\right) & \text{for } L > 0 \end{cases} \quad (13)$$

where $\xi = (1 - 16z/L)^{1/4}$.

The temperature profile is written as follows:

$$T(z) = T_g + \frac{T_*}{\kappa}\left(\ln\left(\frac{z + z_0}{z_0}\right) - \psi_H\right) - \Gamma_d z \quad (14)$$

where $\Gamma_d = 0.011\,\mathrm{Km}^{-1}$ is the dry adiabatic lapse rate and ψ_H is given as follows:

$$\psi_H = \begin{cases} 2\ln\left(\dfrac{1+\xi^2}{2}\right) & \text{for } L < 0 \\ -5\dfrac{z}{L} & \text{for } L > 0 \end{cases} \tag{15}$$

Turbulence profiles on the inlet follow the suggestions of Han et al. (2000). The expressions for neutral and stable atmospheric boundary layers read:

$$k(z) = \begin{cases} 6u_*^2 & \text{for } z \le 0.1h_{abl} \\ 6u_*^2\left(1-\dfrac{z}{h_{abl}}\right)^{1,75} & \text{for } z > 0.1h_{abl} \end{cases}$$

$$\varepsilon(z) = \begin{cases} \dfrac{u_*^3}{\kappa z}\left(1.24+4.3\dfrac{z}{L}\right) & \text{for } z \le 0.1h_{abl} \\ \dfrac{u_*^3}{\kappa z}\left(1.24+4.3\dfrac{z}{L}\right)(1-0.85zh_{abl})^{1.5} & \text{for } z > 0.1h_{abl} \end{cases} \tag{16}$$

h_{abl} is the height of the atmospheric boundary layer, which typical is about 1000–1500 meters for unstable boundary layers. For neutral and stable boundary layers, the boundary layer height is given by the friction velocity u_*, the Coriolis parameter f_c, and the Monin-Obukhov length as follows:

$$\begin{aligned} h_{abl,\mathrm{neutral}} &= 0.3\frac{u_*}{f_c} \\ h_{abl,\mathrm{stable}} &= 0.4\left(\frac{u_*L}{f_c}\right)^{1/2} \end{aligned} \tag{17}$$

In unstable atmospheric boundary layers, there is significant more turbulent kinetic energy than under stable conditions. Heat fluxes from the ground produces vertical flows that increase the turbulence level. These vertical flows are parameterized by a convective velocity scale:

$$w_* = \left(\frac{g\dot{q}_g h_{abl}}{T_0\rho_\infty c_p}\right)^{1/3} \tag{18}$$

where $\dot{q}_g$ is the heat flux from the ground, T_0 and ρ_∞ denote reference temperature and density, respectively. The convective velocity scale is the single most important parameter when determining the turbulence parameters in the atmospheric boundary layer (Han, 2000):

$$k(z) = \begin{cases} 0.36w_*^2 + 0.85u_*^2\left(1-3\dfrac{z}{L}\right)^{2/3} & \text{for } z \le 0.1\,h_{abl} \\ \left(0.36+0.9\left(\dfrac{z}{h_{abl}}\right)^{2/3}\left(1-0.8\dfrac{z}{h_{abl}}\right)^2\right)w_*^2 & \text{for } z > 0.1\,h_{abl} \end{cases}$$

$$\varepsilon(z) = \begin{cases} \dfrac{u_*^3}{\kappa z}\left(1+0.5\left|\dfrac{z}{L}\right|^{2/3}\right)^{1.5} & \text{for } z \le 0.1\,h_{abl} \\ \dfrac{w_*^3}{h_{abl}}\left(0.8-0.3\dfrac{z}{h_{abl}}\right) & \text{for } z > 0.1\,h_{abl} \end{cases} \tag{19}$$

Wind meandering is a critical parameter when comparisons with experimental data for large scale experiments with a certain duration is performed. In FLACS, two time scales, typically of order 10 and 60 seconds can be set and sinus-shaped variations of the wind is obtained on the inlet boundaries. Fluctuations with smaller time scales are included in the turbulent kinetic energy.

Hazardous distance for flammable gases is determined by the distance to the point where the concentration of flammable gas is less than half of the lower flammability limit (LFL/2). Accurate modelling the hazardous distance is sensitive the turbulent diffusion. The turbulence level in the gas plume depends on the wind turbulence that is given on the inlet and the production of turbulent kinetic energy due to density differences between the gas plume and surrounding air. Turbulent production due to buoyancy is usually modelled by:

$$G_{b,S} = -\frac{1}{\rho}\left(\frac{\mu_{eff}}{\sigma_t}\right)g_j\frac{\partial\rho}{\partial x_i} \tag{20}$$

where $\sigma_t = 0.8$ is the turbulent Prandlt number and μ_{eff} is the effective viscosity. Maele & Merci (2006) showed that equation (20) gives too little turbulent kinetic energy for some buoyant plumes and they recommended an alternative expression of Daly & Harlow (1970):

$$G_{b,G} = -\frac{3}{2}\frac{\mu_{eff}}{\sigma_t\bar{\rho}^2\,k}\left(\overline{u_i'u_j'}\frac{\partial\bar{\rho}}{\partial x_i}\right)\rho_\infty g_j \tag{21}$$

BURRO & COYOTE TEST SERIES

EXPERIMENTAL CONDITIONS

Both the Burro and the Coyote test series were performed by Lawrence Livermore National Laboratories on behalf of US Department of Energy at the Naval Weapons Center at China Lake, California. The Burro and Coyote test series were conducted in 1980 and 1981 respectively.

In the Burro series a total of 8 tests with LNG are reported. These tests are extensively described in Koopman et al. (1982). Release rates were of the order 100 kg/s. Wind speeds were mainly ranging from 5 to 9 m/s, except in Test 8 where a much lower wind speed was observed (1.8 m/s). The prevailing wind direction was 225°; generally the observed wind direction in the tests was close to this. Temperatures were from 33–40°C and relative humidity was low (2–12%), i.e. the absolute humidity would be of the order 0.5% or less. Gas concentration was recorded at 25 different locations. The 25 gas sensors were split up into 3 arcs at 57 m, 140 m and 400 m from the spill location. For each location concentration was recorded at up to three elevations (1 m, 3 m and 8 m above ground). The releases were performed centrally in a 58 m diameter shallow pool, with a rim about 1 m above the water level. The release duration varied from 80–190 s.

As mentioned above, the Coyote test series was performed generally in the same conditions as Burro. The

Coyote series consisted in 10 tests that were reported by Goldwire et al. (1983). In an attempt to learn more about Rapid Phase Transitions (RPT), the amounts of ethane and propane in the LNG was higher for Coyote tests (methane fraction was around 80%) than for the Burro tests (methane fraction was mainly around 90%). The Coyote tests 3, 5 and 6 were selected as benchmarks for dispersion model validation. The wind speeds were ranging from 4.6 to 9.7 m/s, the spill rates from 100.7 to 129 kg/s and spill durations from 80 to 110 s. As in the Burro series the prevailing wind direction was 225°. Temperatures were from 24–38 °C and relative humidity from 11–23%. The 25 gas measurement positions were at somewhat modified positions for Coyote (measurement arcs at 140 m, 200 m and 400 m) but the measurement heights were the same.

The Burro and Coyote tests occurred under different atmospheric stability conditions, from very unstable to stable. Measurements of heat flux from the ground were conducted and reported in the description of the experiments. The terrain in the Burro and Coyote series was not totally flat. After the 58 m diameter spill pond the terrain was irregular over 80 m with a rise of 7 m. Beyond this location the terrain was relatively flat.

COMPARISON WITH PREVIOUS FLACS SIMULATIONS

The Burro and Coyote series have been simulated with FLACS using two different approaches for the source term and the representation of the atmospheric stability. In this section the predictions of the approach described in section 2 are compared with those of a simpler approach in which diffusive leaks and a neutral condition have been used to model the evaporation of LNG and atmospheric stability (Hansen, 2007).

In the "simple" approach, diffusive leaks have been used to define the source term. It was assumed that all the LNG released would evaporate almost immediately with a pool diameter of roughly 20 m. Four diffusive leaks have been defined forming a (X) just above the ground level. The temperature of the gas released has been set to the normal boiling point of natural gas (−161.5°C). The release rates were specified according to the experimental data. A neutral (D) atmospheric stability class was specified and the profiles for the turbulent kinetic energy and turbulent dissipation rate were computed with equation (19) at the inlet boundaries. Heat transfer from the ground to the cold plume was not taken into account. The horizontal grid resolution was 2 m in the measurement arrays. The vertical grid resolution was 0.5 m and was stretched above 8 m, i.e. the last measurement position. Finally, equation (20) was used for the turbulent production or dissipation due to buoyancy.

In the approach described in section 2, a two-dimensional transient spill model is solved simultaneously with a three-dimensional transient flow for the wind. The Pasquill classes were set for each of the Burro and Coyote tests according to the reported observations. Measurements of sensible heat flux were also reported and have been used to specify a mean heat flux from the ground in the simulations. The grid resolution in the vertical direction was the same as for the "simple" approach. In the horizontal direction, a 1 m grid cell size has been used in the spill pond and a 2–4 m grid cell size in the measurement arrays. Equation (21) was used for the modelling of turbulent production or dissipation by buoyancy effects. Simulations were also preformed with Equation (20) and little differences were observed, with equation (21) giving the better results when compared to experimental data. The results of the sensitivity study concerning the buoyant turbulent production term will be presented in the next section.

Figure 1 shows the parabola plots obtained with the two approaches. The zero variance line is shown on both plots (i.e. the parabola). A geometric mean larger than 1.0 indicates that the simulation over-predicts the data whereas a geometric mean smaller than 1.0 indicates that the simulation under-predicts the data. The variance gives an estimation of the scatter of the predictions about the data. A point which is close to the zero variance line indicates that the simulation consistently over-predicts or under-predicts the data.

The "simple" approach gives the closest predictions to experimental data. A more detailed discussion on the differences in the results obtained with the two approaches is given in the following. First we consider the Burro tests for which the atmospheric stability was defined as neutral, i.e. the Burro tests 7 and 9. For these tests the predictions of the two approaches are very close, indicating that the different options used to model the source term give very similar results. This verifies the presented pool spread and evaporation models. Therefore, the differences observed on the two parabola plots (considering all the Burro and Coyote tests) are due to the modelling of the atmospheric stability and the turbulent diffusion as well as the heat transfer from the ground to the cold plume. For all the tests but Burro 8, 7, 9 and Coyote 6, the atmospheric boundary layer (ABL) was defined as unstable. In the "simple" approach the ABL was considered neutral for all cases. In an unstable ABL, the level of atmospheric turbulence is increased as compared to a neutral ABL. This increased turbulence level may have two effects: at one given position the concentration in the gas cloud might be lower for an unstable ABL due to mixing with the surrounding air and larger at another given position due to the transport to upper levels by the turbulent eddies. These phenomena are coherent with the observations on Figure 1. An unstable ABL leads to appreciatively a 10% reduction in the maximum predicted concentrations compared to a neutral ABL. Looking closer to the results, one could observe that the reduction in the maximum concentrations is occurring at the two first heights, i.e. 1 m and 3 m, whereas the maximum concentrations are slightly over-estimated at the height of 8 m. This is in turn giving an explanation for the larger variance obtained with the unstable ABL. The Burro 8 test was performed under a stable ABL. Both approaches, using a flat terrain, give unsatisfying results.

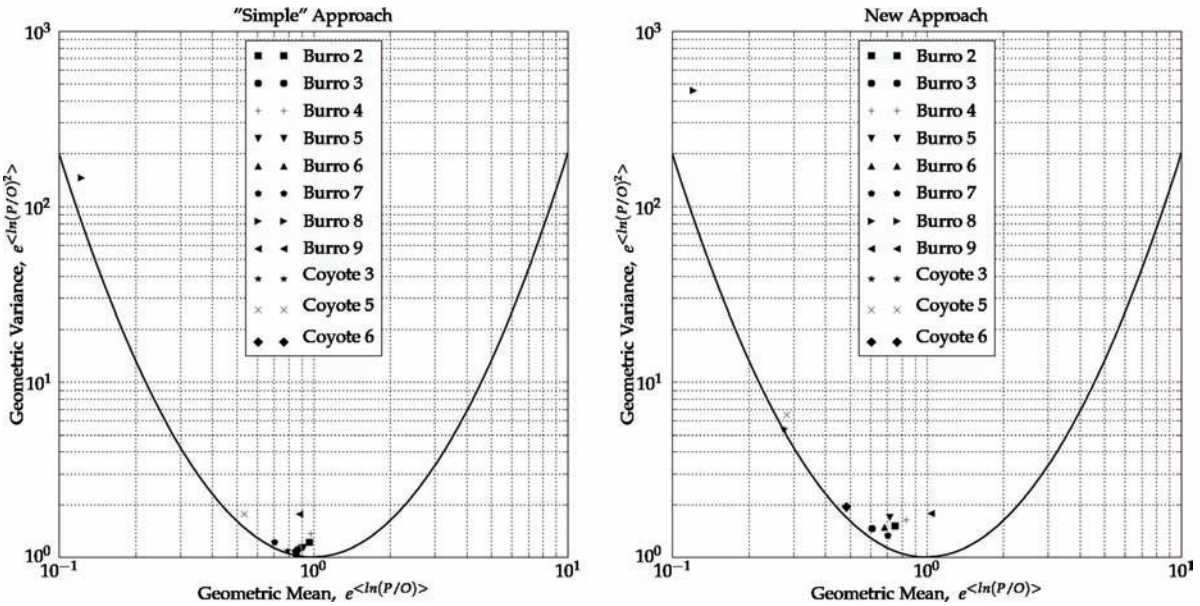

Figure 1. Parabola plots. The predicted (P) and observed (O) maximum concentrations are compared. For the Burro tests, the maximum values at the two first rows (57 m and 140 m) for each height (1 m, 3 m and 8 m) are considered. For the Coyote tests, the maximum values at the three first rows (140 m, 200 m and 400 m) for the two first heights (1 m and 3 m) are considered.

As it will be discussed in the last section, the flat terrain assumption has a non-negligible influence on the Burro 8 test. Finally, the largest differences are observed for the Coyote tests. The Coyote tests 3 and 5 were performed under unstable ABL and Coyote 6 under a neutral ABL. It is worth noting that for these tests the comparison with experimental data was made further downwind compared to the Burro tests and only at the two first heights. These results confirm the previous observations. The rate of mixing of the dense gas cloud with the surrounding air is over-predicted and this over-prediction is increasing with downwind distance. Some elements of discussion on these observations will be given in the conclusions.

SENSITIVITY

A sensitivity study has been performed on the terrain and buoyancy modelling. The results for the terrain sensitivity study will be presented for the Burro 8 test and the results for the buoyancy modelling sensitivity study will be discussed for Burro 3.

As pointed out by several authors, i.e. Koopman et al. (2007), the influence of the terrain was clearly observed in the Burro 8 test. The Burro 8 test was conducted under a stable ABL and with a very low wind speed. Gravity flow, due to density gradients in the horizontal direction, led to the widest cloud of all the tests. As the wind speed was very low, gravity flow was dominating over wind driven flow and then terrain effects were of major importance. The influence of terrain is illustrated on Figure 2. Two simulations with the same grid but with and without the terrain were performed. The time-series of the gas concentration

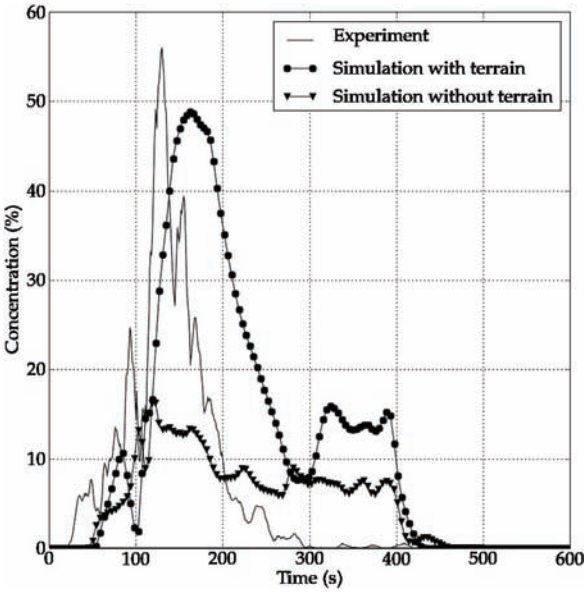

Figure 2. Time-series of gas concentration for Burro 8 at a height of 1 m, 57 m downwind.

57 m downwind of spill point and at a height of 1 m obtained with the two configurations are compared with the experimental data. The influence of the terrain is clearly noticed and explains the very poor results obtained on the parabola plots.

Figure 3 shows the results of the sensitivity study performed for the turbulent buoyant production term. The test

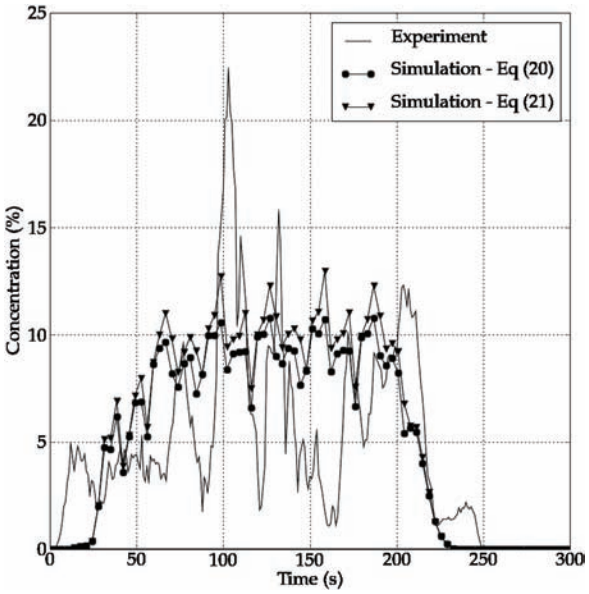

Figure 3. Time-series of gas concentration for Burro 3 at a height of 1 m, 57 m downwind.

Burro 3, performed under unstable atmospheric condition, is used in this sensitivity study. Equations (20) and (21) were used to model the turbulent buoyant production term. The time-series of the gas concentration 57 m downwind of spill point and at a height of 1 m obtained with the two configurations are compared with the experimental data. The expression of Daly & Harlow given by equation (21) gives higher concentration compared to the standard expression, equation (20). This indicates that with the expression of Daly & Harlow stratification effects (presence of the dense gas cloud) dampens more the turbulence than with the standard expression. The expression of Daly & Harlow gives also the closest prediction to the experimental data.

CONCLUSIONS

The FLACS CFD tool has been used to simulate the Burro and Coyote test series. In the present work, a two-dimensional transient spill model was solved simultaneously with a three-dimensional transient flow for the wind. Atmospheric stability was taken into account via the specification of a Pasquill stability class. The predicted concentrations obtained with this new methodology have been compared with the predictions from previous FLACS simulations in which a "simpler" approach had been used, i.e. neutral ABL and diffusive leaks for the source term. The results have also been compared with experimental observations. The results obtained with both the new methodology and the "simple" approach agree relatively well with the experimental observations.

The comparisons have shown that the presented pool spread and evaporation models give reasonably accurate predictions for the source term. The influence and importance of atmospheric stability has been pointed out. In the new methodology, closer to reality, the atmospheric stratification has been modelled. For the tests performed under an unstable ABL, the maximum concentrations were underestimated at the two first measurement heights, i.e. 1 m and 3 m, and over-estimated at a height of 8 m. An explanation for this result could be that the k-ε turbulence model, used in the computations, is not able to handle properly the competing effects and interactions between an unstable, convective, ABL and a dense, stratified, gas cloud. The presence of the dense cloud tends to dampen the turbulence whereas an unstable atmospheric stratification increases the turbulence mixing and vertical transport of scalars. Future work will be in close relation to the understanding and modelling of this complex phenomenon. As regards to the experimental test performed under a stable ABL (Burro 8), the importance of a proper representation of the terrain has been emphasized. A flat terrain assumption led to a large under-prediction of the maximum concentrations.

REFERENCES

Bernatik, A., Libisova, M. 2004, Loss prevention in heavy industry: risk assessment of large gasholder. *J. Loss Prev. Process Ind.*, 17: 271–278.

Bosch, C. J. H. van den, Weterings, R. A. P. M. (Ed), 2005, Methods for the calculation of physical effects – due to releases of hazardous materials, CPR 14E. (TNO Yello Book) 3rd edition, 2nd print, TNO, The Hague, The Netherlands.

Brandeis, J., Kansa, E. J., 1983, Numerical simulation of liquefied fuel spills: I. Instantaneous release into a confined area. *Int. J. Numer. Methods Fluids*, 3: 333–345.

Brandeis, J., Ermak, D. L., 1983, Numerical simulation of liquefied fuel spills: II. Instantaneous and continuous LNG spills on an unconfined water surface. *Int. J. Numer. Methods Fluids*, 3: 346–361.

Carson, P., Mumford, C., 1994, Hazardous chemical handbook, Butterworth, Oxford, U.K.

Conrado, C., Vesovic, V., 2000, The influence of chemical composition on vaporization of LNG and LPG on unconfined water surfaces. *Chem. Eng. Sci*., 55: 4549–4562.

Daly, B. J., Harlow, F. H., 1970, Transport equations in turbulence. *Phys. Fluids*, 13: 2634–2649.

Deaves, D. M., 1992, Dense gas dispersion modelling. *J. Loss Prev. Process Ind.*, 5: 219–227.

European Commission, 2002, Green paper: Towards a European Strategy for the security of Energy Supply; Report COM(2002) 321, Commission of the European Communities, Brussels, Belgium.

Gavelli, F., Bullister, E., Kytomaa, H., 2008, Application of CFD (Fluent) to LNG spills into geometrically complex environments, *J. Hazard. Mat.* 159: 158–168.

GexCon, 2009, FLACS User's Manual, http://www.gexcon.com.

Goldwire, H. C., et al., 1983, Coyote Series Data Report, LLNL/NWC 1981 LNG Spill Tests Dispersion, Vapor Burn, and Rapid Phase Transition, UCID-19953, vols. 1/2.

Han, J., Arya, S. P., Shen, S., Lin, Y.-L., 2000, An estimation of turbulent kinetic energy and energy dissipation rate based on atmospheric boundary similarity theory. Tech. Rep. CR-2000-210298, NASA, USA.

Hansen, O. R., Melheim, J. A., Storvik, I. E., 2007, CFD-modeling of LNG dispersion experiments. In AIChE Spring meeting, Houston, Texas, USA.

Havens, J., 1998, A Dispersion Model for Elevated Dense Gas Jet Chemical Releases, Volume I, EPA-450/4-006a.

Hightower, M., et al., 2004, Guidance on Risk Analysis and Safety implications of a Large Liquified Natural Gas (LNG) Spill Over Water, Sandia National Laboratories Report: SAND2004-6258.

Koopman, R. P., et al., 1982. Analysis of Burro series 40-m3 LNG spill experiments. *J. Hazard. Mater*., 6(1/2): 43–83.

Koopman, R. P., Errmak, D. L., 2007, Lessons learned from LNG safety research. *J. Hazard. Mater*., 140: 412–428.

Maele, K. van, Merci, B., 2006, Application of two buoyancy-modified k-ε turbulence models to different type of buoyant plumes. *Fire Safety J.*, 41: 122–138.

Toro, E. F., 2001, Shock-capturing methods for free-surface shallow water flows. Wiley, UK.

Sklavounos, S., Rigas, F., 2005, Fuel Gas Dispersion under Cryogenic Release Conditions, *Energy Fuels*, 19: 2535–2544.

Ulden, A. P. van, Holtslag, A. A. M., 1985, Estimation of atmospheric boundary layers parameters for diffusion applications. *J. Climate Appl. Met.*, 24: 1196–1207.

Woodward, J. L., 1990, An integrated model for discharge rate, pool spread, and dispersion from punctured process vessels. *J. Loss Prev. Process Ind.*, 3: 33–37.